Paper:
Liao, Z., Yao, X., Zhang, L., Hossain, M., Wang, J. & Zang, S. (2019). Temperature and strain rate dependent large tensile deformation and tensile failure behavior of transparent polyurethane at intermediate strain rates. *International Journal of Impact Engineering, 129*, 152-167.
http://dx.doi.org/10.1016/j.ijimpeng.2019.03.005

Temperature and strain rate dependent large tensile deformation and tensile failure behavior of transparent polyurethane at intermediate strain rates

Zi-Sheng Liao[a], Xiao-Hu Yao[a,*], Long-Hui Zhang[b], Mokarram Hossain[c], Jiong Wang[a,**], Shu-Guang Zang[d]

[a]*School of Civil Engineering and Transportation, South China University of Technology, 510640 Guangzhou, Guangdong, China*
[b]*Faculty of Mechanical Engineering, Technion, 32000 Haifa, Israel*
[c]*Zienkiewicz Centre for Computational Engineering, College of Engineering, Bay Campus, Swansea University, Swansea, UK*
[d]*China Building Material Academy, 100024 Beijing, China*

Abstract

Transparent polyurethane has been widely applied in laminated windshield glasses as the interlayer material to enhance the reliability due to its outstanding impact resistance. Under impact loading such as bird strike, the interlayer undergoes large tensile deformation mainly at intermediate strain rates (at the order of magnitudes from 10^0 to 10^3, excluding 1000 /s). In addition, the interlayer is on service over a wide range of temperatures for a plane traveling around the world. The mechanical behavior of transparent polyurethane under these conditions is not fully understood. In this study, systematical experiments were performed on transparent polyurethane. The viscoelasticity of the material was firstly verified by several quasi-static cyclic tests. Then a series of large tensile deformation and tensile failure experiments were conducted under intermediate strain rates and at temperatures of -40°C to 40°C using a servo-hydraulic high-speed tensile machine. All strain data were acquired by the DIC technique. The experimental results show that tensile stress-strain curves and failure behaviors are significantly

*Corresponding author. Tel.: +86 20-87111030.
**Corresponding author. Tel.: +86 20-87111030-3693.
Email addresses: yaoxh@scut.edu.cn (Xiao-Hu Yao), ctjwang@scut.edu.cn (Jiong Wang)

temperature and strain rate dependent. The rate-temperature equivalence was also observed. Finally, a phenomenological analysis of mechanical quantities of the material was carried out.

Keywords:
Transparent polyurethane, Large tensile deformation, Tensile failure,
Temperature dependence, Strain rate dependence, Intermediate strain rate

1. Introduction

Bird strikes are fatal accidents threatening the safety of aeronautical structures and flight crews, and cause annual commercial loss of $193 million merely in US [1]. A measure to minimize the damage of bird strike is to employ laminated glass as a windshield, which consists of two panes of glass bonded by a polymer interlayer in the simplest case. According to investigations of Larcher et al. [2] and Zhang et al. [3], the impact loading of the laminated glass can be divided into several stages, in each of which the interlayer behaves differently. In the beginning, the whole windshield undergoes bending deformation. The ductile polymer interlayer bears mainly compressive force due to its low shear stiffness. Then the glass panes fail and break into splinters sequentially. At this stage, the unbroken panes of laminate structure can still provide residual strength [4]. As long as all panes fail, the interlayer transforms rapidly into large tensile deformation mode. Finally, the interlayer reaches its strength, indicating the final failure of the whole windshield. Here, the reinforced glass panes provide sufficient strength, while the polymer interlayer joining these panes can reduce stress concentration and serve as an energy dissipative buffer. This ingenious structure design equips laminated glass windshield with outstanding impact resistance and strong safety advantage over the monolithic glass.

In addition to the aforementioned safety performance, the interlayer also plays a key role on diverse attributes of the windshield, such as transparency, sound attenuation, and mitigation of post-fracture glass fallout [5]. To meet these requirements, an appropriate material should be chosen carefully. One favorable choice is transparent polyurethane. Polyurethane is a polymer synthesized from di- or poly-isocyanate and polyol monomers. This material is phase segregated by soft and hard segments. The nonpolar soft segments form the amorphous soft domains, serving as the matrix, while the polar hard segments form the stiff hard domains, acting as crosslinks [6]. Un-

der loading conditions, the soft segments uncoil and the hard segments are aligned and produce strong hydrogen force, which contributes to the high tensile strength and ultimate elongation [7, 8]. These two kinds of incompatible segments provide versatile properties based on stoichiometric variation [9, 10]. The transparent polyurethane discussed in this paper possesses well elasticity with large deformation capacity, well viscosity with large hysteretic loop, strong impact resistance, low glass transition temperature, firm adhesion, sufficient light transmittance, and so forth. These excellent properties contribute to more extensive applications of transparent polyurethane than many conventional interlayer materials.

Structural design is an effective mean to exploit the advantages of laminated glass to the full, which bases on a thorough understanding of involved material such as polyurethane. Under impact loading such as bird strike, the material is in certain conditions. Normally the material is subjected to the loading at intermediate strain rates, which are at the order of magnitudes from 10^0 to 10^3 /s (excluding 1000 /s), i.e. 1 /s to 999 /s. For example, according to experimental results from Yao et al. [11, 12], the speeds of bird strike on aircraft generally ranged from 70 m/s to 250 m/s, which results in strain rate of 10^0 /s to 10^1 /s loaded on the structure. Besides, according to Larcher et al. [2], under a blast loading, the interlayer material of laminated glass was at strain rates from 30 /s to 100 /s. Before a laminated structure fails, the polyurethane interlayer is subjected to large tensile deformation. Moreover, since aircraft travel at various altitudes and coordinates, the laminated windshields are on service over a relatively wide range of temperature. Similar to many polymers, polyurethane shows strong strain rate and temperature sensitivity. Taking these factors into account, investigations on large tensile deformation and tensile failure behavior of transparent polyurethane at various intermediate strain rates and temperatures are essential.

Over the last decades, various experimental investigations have been carried out on polyurethane and the similar material, polyurea. Most of them were compression tests. An early high strain rate split Hopkinson pressure bar (SHPB) test on polyurethane at a single strain rate of 1612 /s was conducted by Sharma et al. [13]. Qi and Boyce [6] carried out continuous and multi-step quasi-static compression cyclic loading tests, and discovered strong hysteresis and softening behaviors of polyurethane. Yi et al. [14] studied compressive properties on both polyurethane and polyurea at strain rates from 10^3 /s to 10^4 /s using SHPB, and reported that materials transform from rubber-like behavior at low strain rates to leather-like or glass-like behavior

at high strain rates. Amirkhizi et el. [15] performed high strain rate confined and unconfined compression tests over 0°C to 40°C, showing the temperature and pressure dependence of polyurethane. Sarva et al. [16] investigated compressive mechanical behavior on both polyurea and polyurethane with various test techniques, verifying the rate dependence at strain rates of 10^{-3} /s to 10^{3} /s. Shim and Mohr [17] also probed into compressive mechanical properties of polyurea at low and high strain rates with both conventional and modified SHPB. Grujicic et al. [18] reported the pressure-shear plate impact testing at very high strain rates (10^{5} /s to 10^{6} /s). Recently, Guo et al. [19] reported compressive strain rate, temperature, and pressure sensitivity of polyurea at strain rates up to 12000 /s.

Contrastingly, only a few reports on the tensile behavior are available. Most of them are about low strain rate or high strain rate tests. Rinaldi et al. [20, 21] investigated the influence of stoichiometry of transparent poly(urethane urea)s on the quasi-static behavior and applied a series of experiments to study the quasi-static tensile behavior of polyurea to strain near 1.2 at low strain rates of 0.003 /s and 0.005 /s. J.T. Fan et al. [22] carried out split Hopkinson tension bar (SHTB) tests at high strain rate from 600 /s to 3800 /s on a polyurethane elastomeric material, and then estimated the failure surface of it by scanning electron microscope (SEM). Zhang et al. [23] reported quasi-static tensile tests in a hydraulically driven system at 0.1 /s and 0.01 /s and high strain rate SHTB tests from 2200 /s to 6500 /s, combining temperature effect over −40°C to 50°C. There are very few works about intermediate strain rate tests. Roland et al. [24] carried out a uniaxial tensile test at strain rate from (0.15 /s to 573 /s) using a drop weight device. Raman et al. [25] carried out tensile failure tests for polyurea from 0.006 /s to 388 /s. Mott et al. [26] investigated the thermal response of polyurea stretched to failure at strain rates from 0.026 /s to 400 /s. However, except for [23], most of these tests were carried out at ambient temperature, while [23] did not involve the intermediate strain rate tests as well as the large deformation and failure behavior.

Overall, even though the compression properties of polyurea and polyurethane have been investigated at full length, studies of tensile properties are still insufficient. The conventional tension apparatuses, such as the universal testing machine, are mainly employed for quasi-static tests at low strain rates, i.e. lower than 1 /s (the order of magnitudes lower than 10^{0} /s), while the SHTB system is mainly applied for high strain rate tests, i.e. greater than 1000 /s (mainly the order of magnitudes 10^{3} and 10^{4} /s). In

addition, the drop weight device and the SHTB are also difficult to achieve stable strain rates. Although most polymers are temperature sensitive, there were also few works about the temperature influence on the dynamic tensile response of polyurethane. Moreover, most studies reported on the polyurea rather than transparent polyurethane. Although these two materials have a similar microstructure, they are different chemicals which require different investigations.

In order to make up the deficiency of available researches and provide data for laminated glass design, in this study, systematical experiments of transparent polyurethane were carried out. Uniaxial dynamic tensile behavior was performed on a high-speed tensile machine to probe into the strain rate and temperature dependence and failure behavior at intermediate strain rates. Several quasi-static cyclic loading tests mentioned in [6] were conducted to verify the viscoelasticity and cyclic mechanical behaviors. A phenomenological analysis on initial modulus, pseudo yield point, pseudo lower yield point, secondary modulus, and tensile failure point was carried out.

2. Experimental details

2.1. Materials and specimens

In this study, S-123 transparent polyurethane provided by the company PPG was investigated, which was the same material as researched by Zhang et al. [23, 27]. The material was based on dicyclohexylmethylmethane-4,4-diisocyanate (HMDI), and polytetramethylene ether glycol (PTEG). The light transmittance was over 90% and the density was 1180 kg·m^{-3}. According to the DMA tests in [23], the glass transition temperature of the polymer is around -40C to -30C.

As in most cases of tensile failure tests, our specimens were designed in flat dumbbell shape in case they broke in the grippers. We had two designs of specimens. The first design (Fig. 1(a)) had a 5 mm gauge section (the central parallel section) and a 2.5 mm fillet radius of the arc section. The second design (Fig. 1(b)) had a 10 mm longer gauge section and a 10 mm fillet radius of the arc section. Both specimens were 3 mm in thickness and 6 mm in width. The dimension errors fell within ±0.3 mm, which were measured by a caliper.

The specimens with a short gauge section were adopted for both quasi-static and dynamic tests. It was designed similar to the one in [23]. The

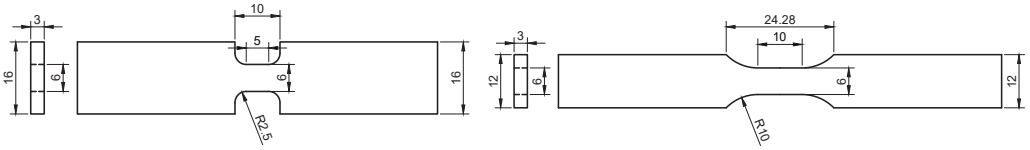

Figure 1. Dimension of specimen (in mm). (a) short specimen with 5 mm gauge section for both quasi-static tests and dynamic tests, (b) long specimen with 10 mm gauge section for dynamic tensile failure tests.

relatively short length could assure the stress equilibrium in the gauge section according to [3]. The arc section with a short fillet radius was desirable to localize the actual deformation in the gauge section. However, the large curvature in this fillet would induce stress concentration and triaxial stress states and consequently influence the strain rate constancy of the gauge section and the measurement accuracy of tensile strength. Hence the second specimens with longer gauge section and larger fillet radius were adopted specially for failure tests and analysis. The arc section was also longer to ensure sufficient width of the grip section since comparable widths of the gauge and the grip section tend to break in the grippers. This long specimen could obtain similar but more stable strain rates at the same tensile speeds in comparison to the short specimen, as shown in Fig. 7(a). Generally, lengthening the specimen can improve strain homogeneity and strain rate constancy within the gauge section.

Given that the ductile polyurethane could produce ultimate elongation up to 300% in certain conditions, both specimen designs were relatively short to ensure that the specimens deformed and broke within the camera coverage and the travel limit of the test machine.

2.2. Quasi-static test system

Quasi-static tensile experiments were conducted on an Instron 5567 universal testing machine. Note that in quasi-static tests, the low strain rate loading induced more compliant behavior of the specimens than in dynamic tests. As a consequence, the specimens were hard to be gripped tightly. To tackle this problem, specimens were bonded to aluminum shims with glue before being mounted to the grippers.

Figure 2. Zwick/Roell HTM-2512 servo-hydraulic dynamic tensile machine and i-SPEED 726 high speed camera.

2.3. Dynamic tensile test system

In this study, the tensile experiments at intermediate strain rates were performed on a Zwick/Roell HTM-2512 servo-hydraulic dynamic tensile machine as shown in Fig. 2, in KINGFA Ltd, Guangzhou, China. The largest tensile force is up to 25 kN and the travel limit is 300 mm. The tensile force is measured by the inbuilt piezo-electric load cell in the crosshead. There is an embedded transducer to measure the displacement of the gripper. Thanks to the hydraulic system, the test machine can maintain constant stretching speeds available from 0.03 m/s to 12 m/s. The speeds covered the corresponding intermediate strain rates from 10^0 /s to 10^2 /s for our specimens. By contrast, conventional tension apparatuses such as universal testing machine and SHTB are unable to cover the intermediate strain rates. The limitations of conventional testing apparatuses rendered our application of servo-hydraulic tensile machine valuable.

2.4. Temperature conditioning device

In order to explore the temperature effects on mechanical behaviors of transparent polyurethane, a temperature conditioning device was utilized, which can regulate the temperature from -100°C to 250°C. The temperature chamber cooled down the environment to a low temperature by the liquid nitrogen vaporization, while heated it to a high temperature by an electric resistance wire, and the cooled or heated gas was then circulated by

a fan. A set of inbuilt thermocouples monitored the chamber temperature and gave feedback signal for the temperature regulation. All specimens were pre-conditioned in a separate temperature chamber at a target temperature overnight (over 10 hours) to ensure a homogeneous temperature in the specimen. Before loading, each specimen was mounted to the grips and kept at the target temperature for 10 to 20 mins. This period could ensure that the temperature inside the chamber was constant, and avoided the specimens being overheated at high temperatures. Note that we had excluded some test results at 40°C where specimens crept before loading at unexpected high temperatures heated by metal grippers.

2.5. Digital image correlation technique

The dumbbell shape of specimens mentioned in Sec. 2.1 would inevitably introduce additional deformation outside the gauge section. Therefore, the inbuilt movement transducer only sampled the relative displacement between the upper and lower grippers instead of the deformation of the gauge section. In this study, all strains and strain rates in both quasi-static and dynamic tests were measured and processed by the DIC (Digital Image Correlation) technique. A high-speed camera IX i-SPEED 726 with a frame speed up to 12500 fps at 1080p resolution was employed to capture the high-speed deformation images of specimens for the DIC analysis. The GOM correlate 2017[1] was employed for the DIC analysis.

Spray paint with a considerable deformation capacity was applied to ensure that sprayed speckles can move and deform along with the surface. During testing, the camera captured the speckle pattern attached to the surface of a specimen, as shown in Fig. 3. Using the DIC technique, the positions of the speckles were tracked to obtain the displacement field at every concerned time interval. Based on this displacement field, the deformation gradient was obtained, and the strain field was subsequently calculated. For a specimen tested at 1 m/s and 25C, the strain distribution at a large overall strain is relatively homogeneous, as shown in Fig. 4. The strain history curves at randomly selected points in the strain field (such as green points G1 to G7 in Fig. 5) and their mean value (adopted as the representative strain history of the specimen) are shown in Fig. 6.

For the dynamic tests, the strain rate decrease of the gauge section over

[1] https://www.gom.com/

Figure 3. A specimen sprayed with speckle.

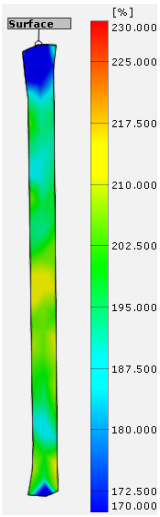

Figure 4. Axial strain distribution in the gauge section at strain around 2.0.

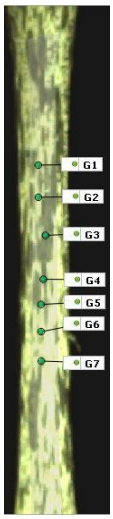

Figure 5. Selected points (green points) for strain history acquisition.

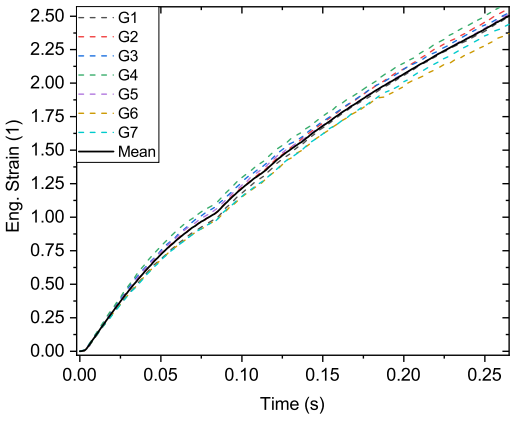

Figure 6. Axial engineering strain history of selected points.

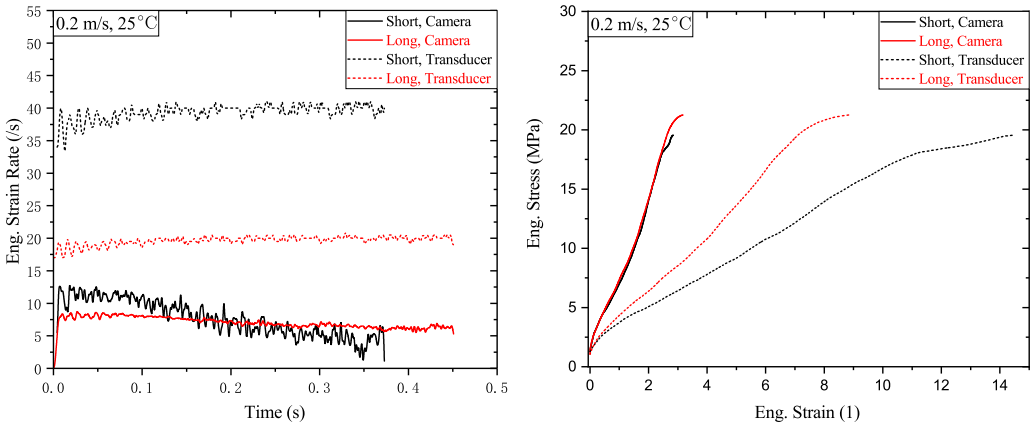

Figure 7. Comparison between the test results measured by camera and by transducer for both short and long specimens. (a) engineering strain rate history curves, (b) engineering stress-strain curves.

time were observed. This was attributed to the deformation of the arc section. Fig. 7 depicts the tests on a short specimen (in back line) and a long specimen (in red line). Both two tests were stretched at 0.2 m/s and ambient temperature. When measured by the DIC technique and camera (in full line), the strain rates of both specimens (in Fig. 7(a)) were actually at around 7 /s. Meanwhile, the corresponding strain-stress curves of two tests (in Fig. 7(b)) were almost overlapped, consistent with the fact that both tests were at similar strain rates. If it is measured by the inbuilt transducer (in dotted lines), we could not exclude the deformation of the arc section. Consequently, the strain rates (in Fig. 7(a)) and strains (in Fig. 7(b)) were overestimated, much larger than the actual results. All these dramatic disparities illustrate the significance of applying the DIC technique.

3. Results

Results of both quasi-static cyclic loading tests and dynamic tests are presented in this section. Engineering stress data were obtained by F/A_0, where F denotes the stretch force and A_0 denotes the initial cross section area of a specimen. Engineering strain data were obtained through the DIC technique as discussed in Sec. 2.5. As a common practice, the results were mainly described in true stress and true strain. Since polyurethane is well

known as a nearly incompressible material, the Poisson's ratio was taken as 0.5. Accordingly, the converting relationship is given by

$$\varepsilon_{\text{true}} = \ln(1 + \varepsilon_{\text{eng.}}) \tag{1a}$$

$$\sigma_{\text{true}} = \sigma_{\text{eng.}}(1 + \varepsilon_{\text{eng.}}) \tag{1b}$$

where $\varepsilon_{\text{true}}$ and $\varepsilon_{\text{eng.}}$ are the true and the engineering strains, respectively. Similarly, σ_{true} and $\sigma_{\text{eng.}}$ are the true and the engineering stresses, respectively.

3.1. Quasi-static cyclic tests

The unloading behaviors of elasticity, viscoelasticity, plasticity, and viscoplasticity are distinctly different from each other. In order to distinguish which property the transparent polyurethane belongs to, tests including not only the loading path but also the unloading path are required. To this end, quasi-static tensile cyclic tests were conducted, including tests of hysteresis, strain softening and equilibrium path as mentioned in [6]. All tests were loaded and unloaded at the speed of 0.05 mm/s, which turned out to be at the strain rate of 0.005 /s. The aforementioned short specimen (Fig. 1(a)) was adopted. These tests did not involve tensile failure. Therefore little error was introduced.

3.1.1. Hysteresis

Fig. 8 shows the true stress-strain curves of uniaxial tensile loading-unloading tests for two specimens stretched to the maximum true strain of 0.41 and 0.69 (corresponding to engineering strains of 0.5 and 1.0, respectively). It is shown that the tensile curves begin with a stiff response, immediately followed by a transition to a lower stiffness, and then slightly harden with strain. The deviation between loading and unloading paths demonstrates the hysteresis behavior of polyurethane. The larger hysteresis and larger residual strain ensue from a larger maximum engineering strain, indicating that hysteresis and residual strain are strain dependent.

3.1.2. Softening

Fig. 9 shows the true stress-strain curve of a continuous cyclic test with three cycles loaded to the same maximum true strain of 0.41 (engineering strain of 0.5). Between each cycle, specimens were maintained in the stress-free state for 200 s to recover the immediate residual strain. Apparently,

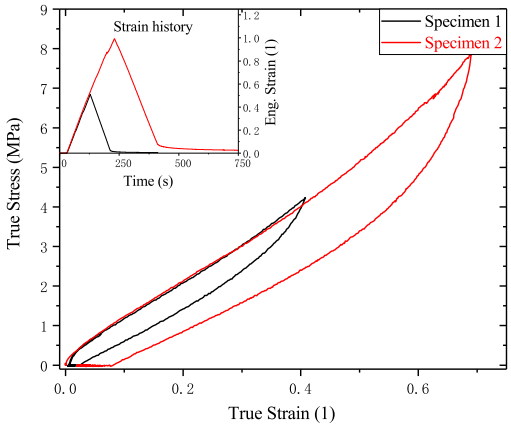

Figure 8. True stress-strain curves of two continuous cyclic tests at $\dot{\varepsilon}_{\text{eng.}} = 0.005$ /s.

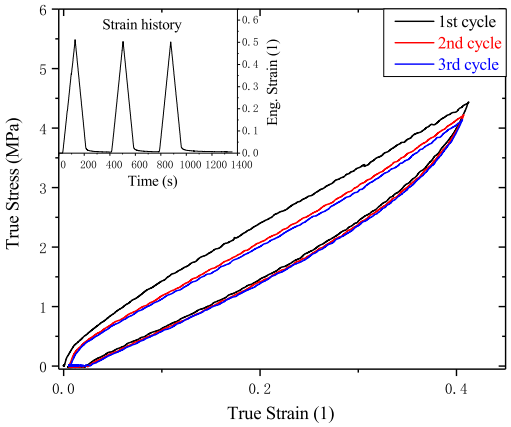

Figure 9. True stress-strain curve of constant strain amplitude continuous cyclic test with three cycles at $\dot{\varepsilon}_{\text{eng.}} = 0.005$ /s.

the second cycle shows a more compliant behavior than the first cycle, while no obvious softening is observed in the third cycle, indicating that softening mainly happens in the first cycle. All three cycles unload through almost the same path.

Fig. 9 also shows that the stress level tends to approach the maximum stress in the previous cycle when the current strain approaches the previous maximum strain. This effect is more apparent in Fig. 10, where specimens were loaded to sequentially increased maximum true strain of 0.41, 0.69 and 0.92 (corresponding to the engineering strain of 0.5, 1.0 and 1.5, respectively) and were rested in the stress-free state for 200 s between cycles. When the specimen in the second cycle was stretched to the maximum strain 0.41 in the first cycle, the stress approached the previous one. As strain increased to the maximum strain of 0.69 in the second cycle, softening took place including the strain of 0.41, as can be seen in the third cycle. Nevertheless, the stress of the third cycle reached almost the same level at strain 0.69. All these features illustrate that softening behavior is strain history dependent. This softening behavior is also known as the Mullins effect [28].

3.1.3. Equilibrium paths

A multi-step cyclic test with 2 cycles (in full line) was conducted (Fig. 11). As shown in the inset, the specimen was relaxed for 100 s at every 0.2 engineering strain increment. The results show that stress decreases in the

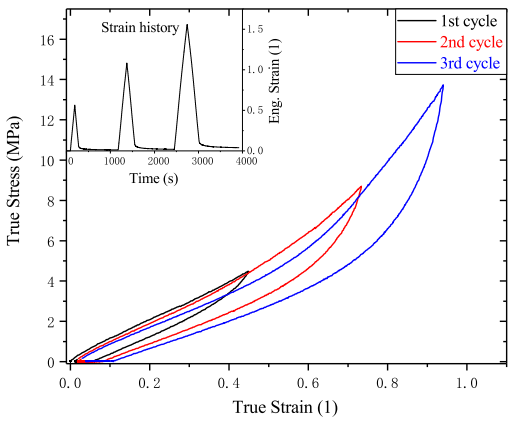

Figure 10. True stress-strain curve of variable strain amplitude continuous cyclic test with three cycles at $\dot{\varepsilon}_{\text{eng.}} = 0.005$ /s.

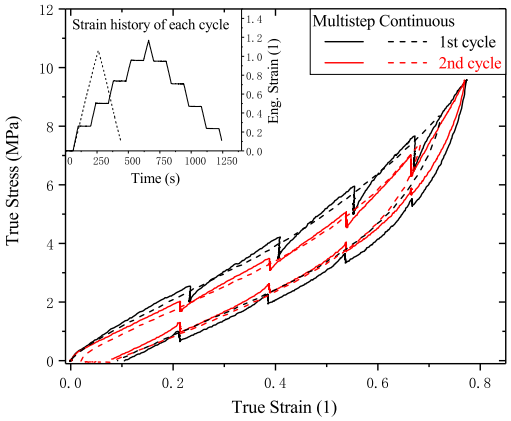

Figure 11. True stress-strain curve of multistep cyclic test with two cycle at $\dot{\varepsilon}_{\text{eng.}} = 0.005$ /s compared with continuous cyclic test with two cycle.

loading path and increases in the unloading path at the relaxation intervals. Suppose that this holding time is extended to a long enough time, the stresses after relaxation at the same strain in loading and unloading paths tend to converge on the so-called equilibrium path [6]. Besides, after the first multi-step cycle (in black), the stress after relaxation approaches closer to the equilibrium path in the second cycle (in red) because of softening. In contrast, the continuous cyclic curves (in dash line) approximately serve as the envelope of the multi-step curves in the corresponding cycle, similar to the result in [17]. Note that due to the slight material behavior and size difference between specimens and due to the deviation of the actual gauge section strain from the target, the continuous cyclic curve appears to go through the curve of multi-step.

In general, the loading-unloading can be regarded as the combination of the equilibrium path and strain history dependent hysteresis. Note that the residual strains could recover without observed permanent set as shown in Fig. 8, Fig. 9 and Fig. 10. Even after failure in dynamic tests in the following discussion, the gauge section recovered to its original length when measured by a caliper. Accordingly, the property of polyurethane is regarded as viscoelastic rather than plastic or viscoplastic.

3.2. Dynamic tensile tests at intermediate strain rates

In this section, the results of dynamic tests at intermediate strain rates are demonstrated. We mainly adopted the long specimens (Fig. 1(b)) for the large deformation and failure tests. Tests of the short specimen (Fig. 1(a)) were conducted for comparison with the previous work by Zhang et al. [23]. Despite the fluctuating temperature and declining strain rate, results show reproducibility even between long and short specimens with different dimensions, which means that the error is relatively small. The tests were carried out at tensile speeds of 0.2 m/s, 1 m/s and 5 m/s, corresponding to the intermediate strain rates at about 7 /s, 50 /s and 300 /s, respectively. The test temperature were at $-40°C$, $-20°C$, $0°C$, $25°C$ and $40°C$.

3.2.1. Load history

An oscillation is observed in the load history curve of high tensile speed tests as shown in Fig. 12. In addition to random noise with a Gaussian distribution, i.e. the Gaussian noise, another reason was the inertia force of lower grippers introduced during speed regulation. Nevertheless, as described in [3], inertia force is also random and fluctuates around the actual force. Therefore, both these two factors were eliminated through data filtering and smoothing. Besides, wave effect also contributed to the oscillation exclusively in dynamic tests. This effect was mitigated by adopting relatively short specimens, which ensured enough round trips of stress wave to reach specimen stress equilibrium.

Fig. 12 shows that stress drops drastically when the specimen failure occurs. For the sake of clarity, the stress-strain curve shown in the following section does not plot the data after the failure.

3.2.2. Strain rate dependence

Each figure in Fig. 13 shows the true stress-strain response at different strain rates and at a certain temperature. As mentioned in Sec. 2.5, at a similar strain rate, the long and short specimens had nearly the same mechanical response except for the failure point. Therefore, the results of short specimens are reliable within a certain strain. Fig. 14 plots the test results of short specimens within true strain $\varepsilon_{\text{true}} = 1$ in comparison to high strain rate and low strain rate tests in [23]. Note that these high strain rate tests and quasi-static tests were not done to break due to experimental limitation. Corresponding test conditions are shown in the legend. In Fig. 14,

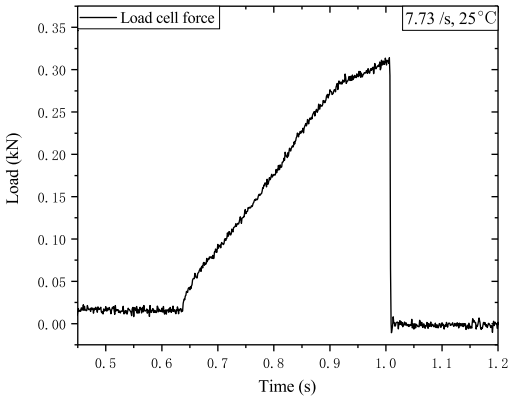

Figure 12. Load history curve of a intermediate strain rate test

curves of our intermediate strain rate tests (in full line) mainly fall between curves of high strain rate and low strain rate tests in [23] (in dash line).

As can be seen in these figures, transparent polyurethane possesses a significant strain rate dependence. At each temperature, overall stress level and initial stiffness increase with the increase of strain rates. At low strain rates, the material behaves as rubber. The stress-strain curves are smooth with a steadily increasing slope. In contrast, at higher strain rates, the material exhibits a yield-like behavior and behaves as leather or glass, consistent with [14]. The stress-strain curves have a steeper initial modulus but then experiences a rollover to a lower modulus. After that, the stress continues to flow just as at lower strain rates until failure.

Note that the polyurethane is not plastic or viscoplastic. Therefore, the turning point in the yield-like curve is just a so-called pseudo yield point [3], after which there is no plastic deformation involved, similar to polyvinyl butyral (PVB). Similarly, the local valley after the pseudo (upper) yield point is called pseudo lower yield point. The material exhibits a more vivid yield-like behavior with a higher pseudo yield strength and a more apparent lower yield point at a higher strain rate. In addition, the failure point is also strain rate sensitive. It is shown that with the increase of strain rate, the tensile strength increases and failure elongation decreases.

3.2.3. Temperature dependence

Each figure in Fig. 15 shows the true stress-strain relationship at different temperatures varying from $-40°C$ to $40°C$ and at the same tensile speed, corresponding to a similar strain rate. It can be observed that with the

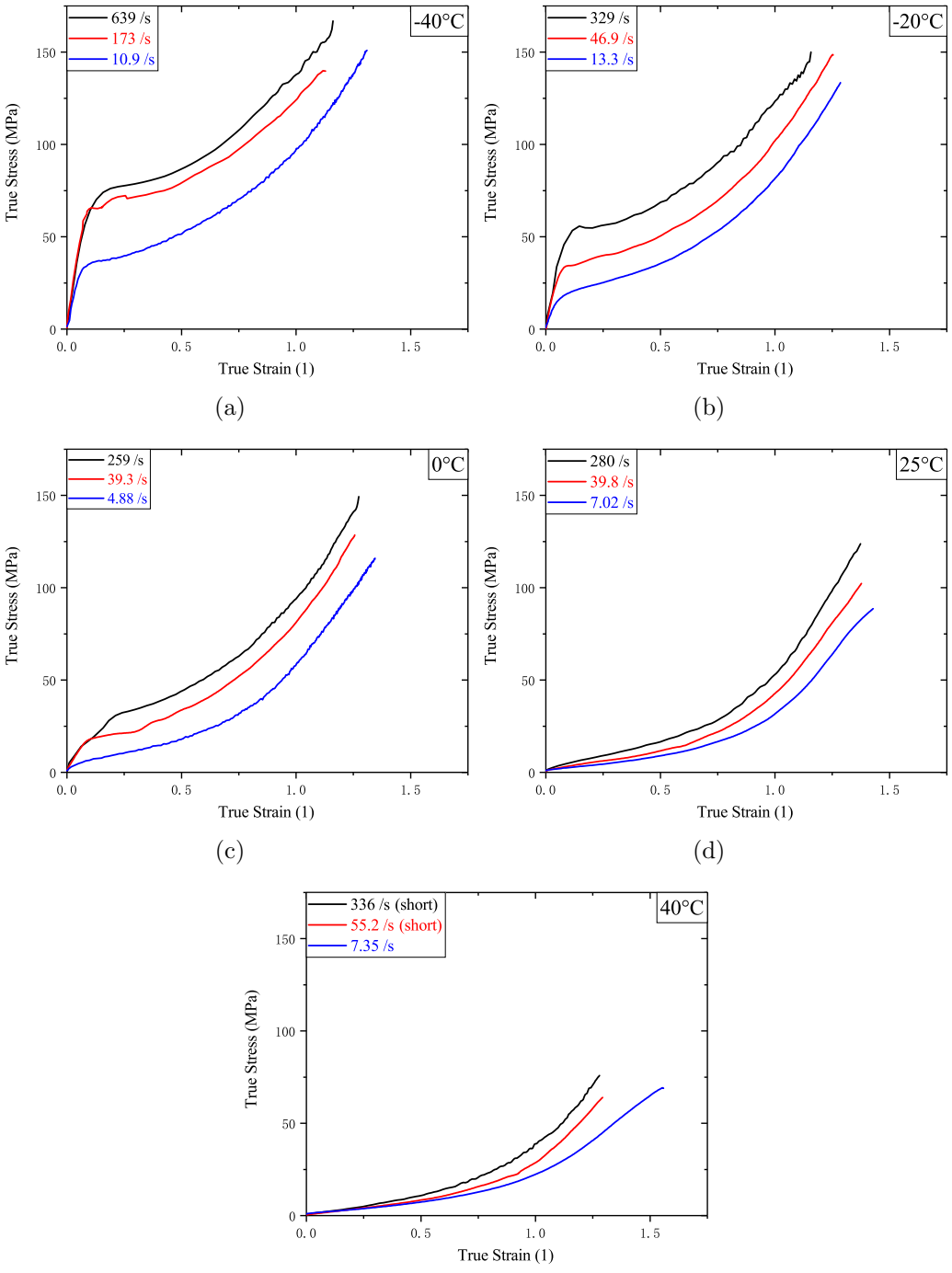

Figure 13. True stress-strain curves at different strain rates and at a certain temperature. (a) −40°C, (b) −20°C, (c) 0°C, (d) 25°C, (e) 40°C.

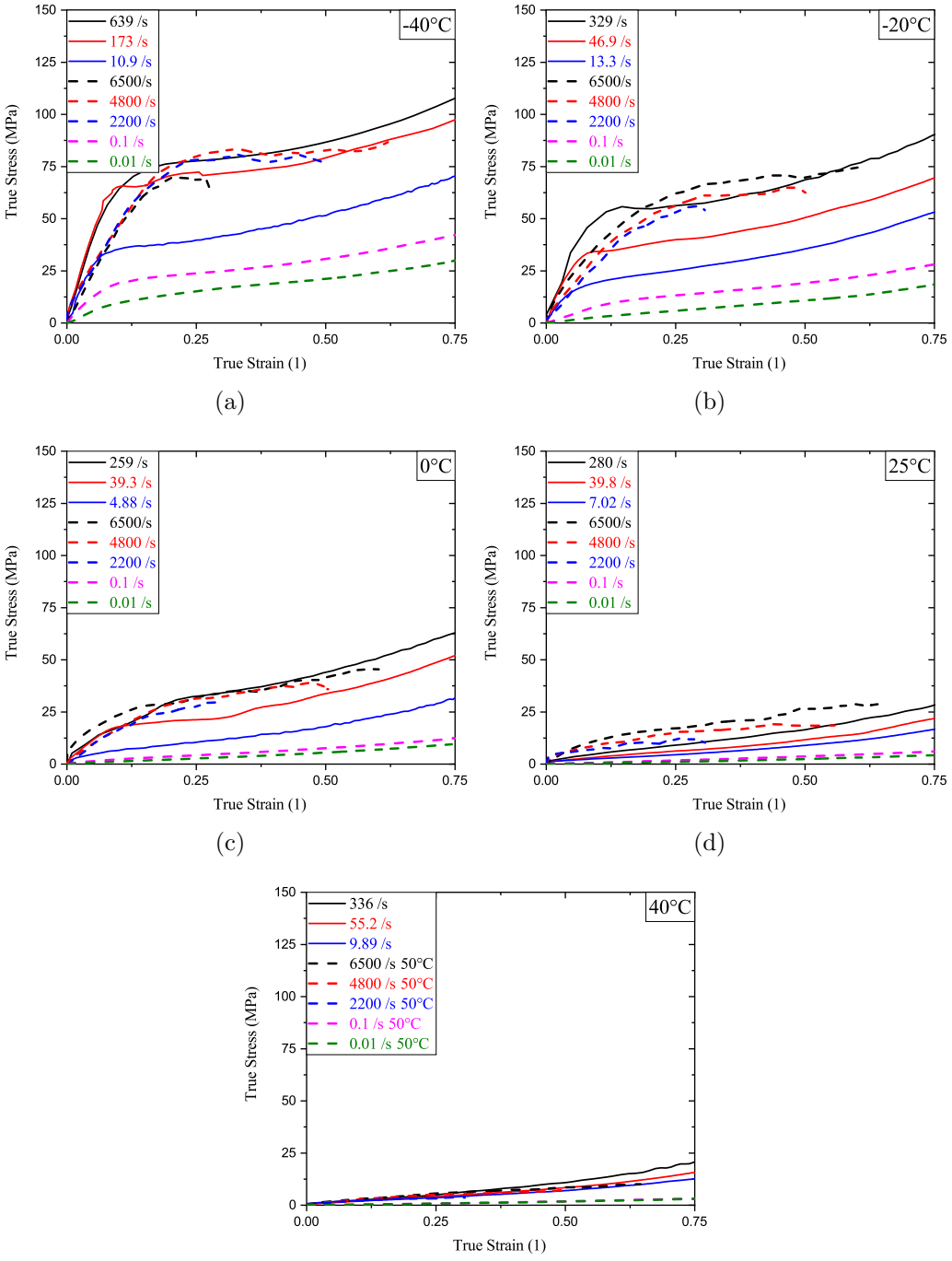

Figure 14. True stress-strain curves at different strain rates and at a certain temperature for short specimen compared to results in [27]. (a) −40°C, (b) −20°C, (c) 0°C, (d) 25°C, (e) 40°C.

temperature decrease, the stress level increases significantly. This is similar to the influence of the increase of strain rate. At higher temperatures of 25°C and 40°C, the stress-strain curves also exhibit a rubber-like behavior. At lower temperatures below 0°C, the material begins to transition into leather-like behavior with a steep initial modulus and a yield-like rollover to a lower modulus. Colder temperatures even bring about the stress drop before stress hardening similar to glass.

With better and clearer presentations, some experimental results were illustrated in the engineering stress-strain forms in the literature [3, 29]. We also plotted the engineering curves for comparison. The temperature effect on mechanical behavior can be observed more clearly in engineering stress-strain curves as shown in Fig. 16. When the temperature decreases from 40°C to −40°C, the initial modulus and yield stress increases drastically. After the pseudo yield point, stress hardens at a higher temperature, and the stiffness strengthens with the increase of temperature at the beginning. However, when the temperature is below 0°C, the yield point stands out, followed by a stress drop. At this stage, the lower yield point appears, and then the hardening stiffness begins to weaken. At −40°C, material instability even occurs.

From the results above, it is clear that the mechanical behavior is determined by both the temperatures and the strain rates. One may notice that the increase of strain rate has the same effect on polyurethane as the decrease of temperature, and vice versa. Both the temperature decrease and the strain rate increase cause the growth of initial modulus and pseudo yield stress, and cause the rise and then fall of the secondary modulus, i.e. the slope of the linear segment following the pseudo lower yield point. In addition, both temperature decrease and strain rate increase induce the transition from a rubber-like behavior to a glass-like behavior. This is a common phenomenon of polymers called the rate-temperature or time-temperature equivalence. In the following Sec. 4.1, this issue is discussed in detail.

4. Analysis

In this section, a phenomenological analysis is conducted. Mechanical quantities of transparent polyurethane are fitted with empirical fitting functions. These functions are mathematically simple with a few parameters. Therefore they are easy to understand and are practical for engineering applications. This analysis can reveal the overall characteristics of the material

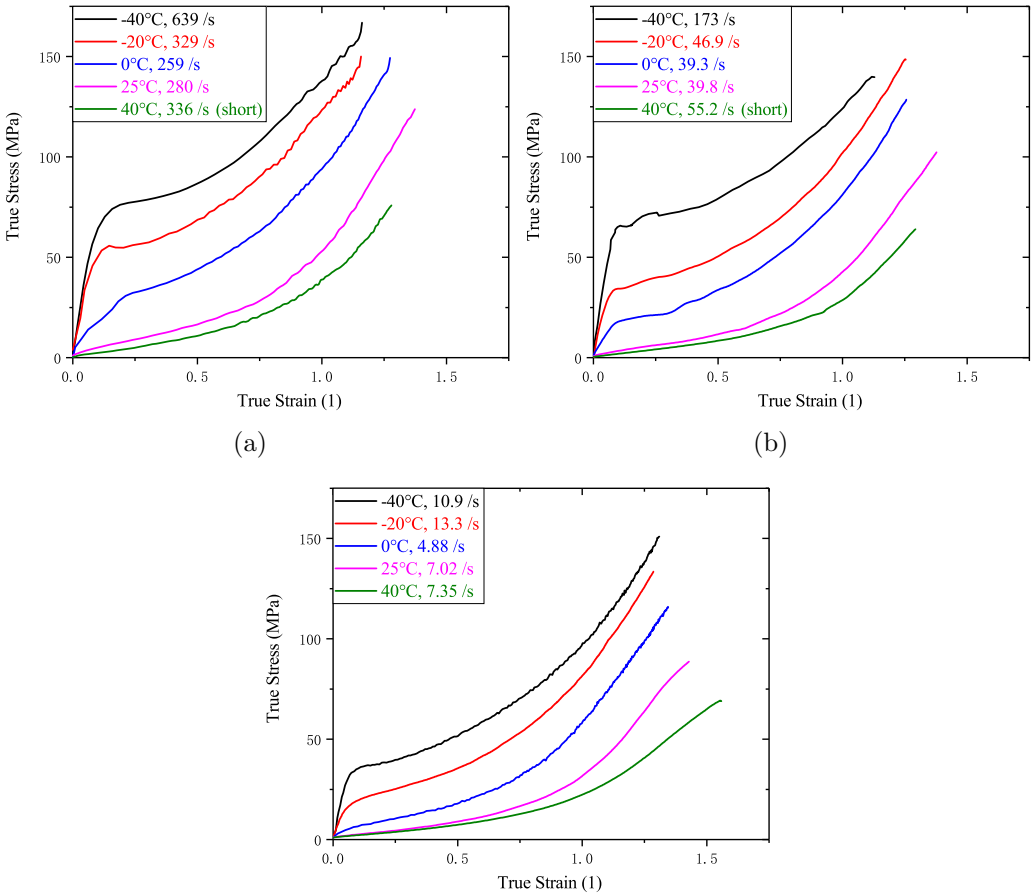

Figure 15. True stress-strain curves at specific strain rates and different temperatures. (a) around 300 /s, (b) around 50 /s, (c) around 7 /s.

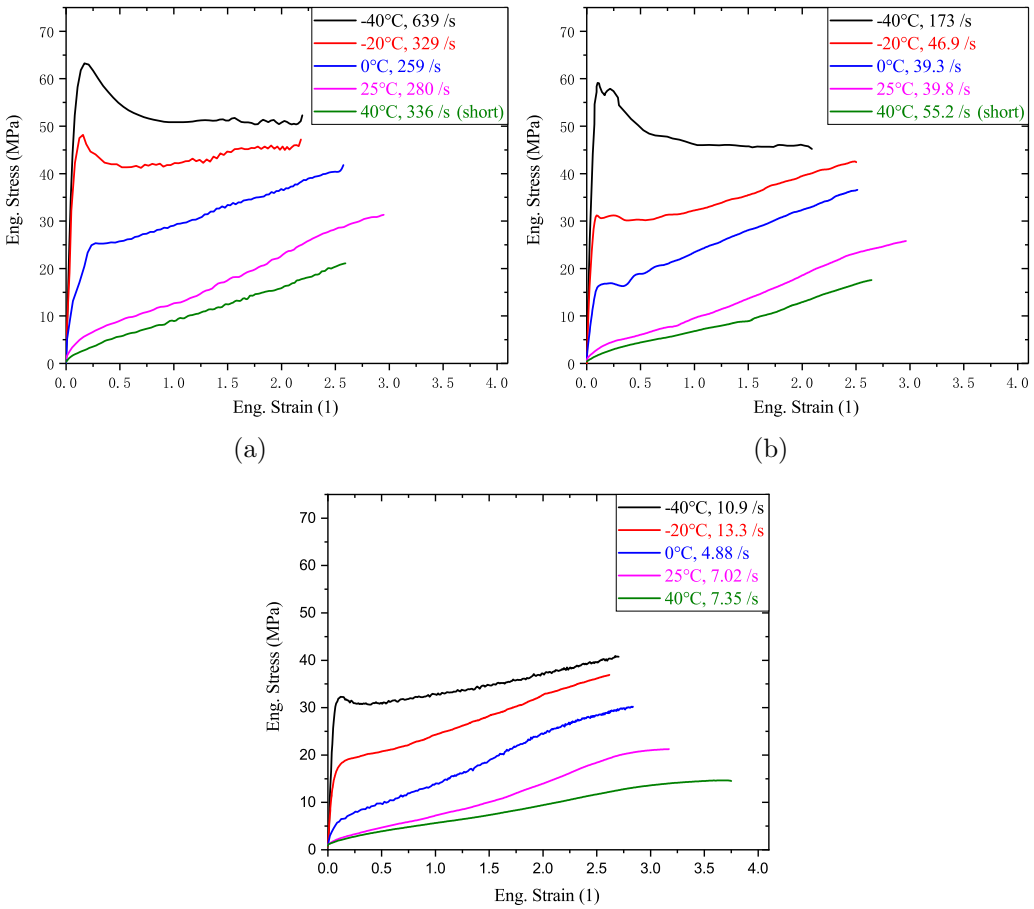

Figure 16. Engineering stress-strain curves at specific strain rates and different temperatures. (a) around 300 /s, (b) around 50 /s, (c) around 7 /s.

and the effect of factors such as strain rate and temperature in the quality sense, and guide us to develop constitutive models.

In the following sections, the time-temperature superposition principle and mechanical quantities of polyurethane including initial modulus, pseudo (upper) yield stress and strain, pseudo lower yield stress and strain, tensile strength, and ultimate elongation are discussed. Here we adopt engineering stress and strain to describe these quantities since some mechanical behaviors are more natural to describe in the engineering form. It is not difficult to convert the results from engineering stress and strain into the true ones using Eq. 1 if necessary. As for the curves of mechanical quantities concerning strain rate, logarithmic strain rate axis is adopted. Data of the short and long specimens are applied together for analysis.

4.1. Time-temperature superposition principle

The results of the dynamic tests in Sec. 3.2 show that the temperature decrease effect and the strain rate increase effect bear resemblance. This is a common phenomenon of polymers called rate-temperature or time-temperature equivalence, as a higher strain rate indicates a shorter relaxation time. When temperature decreases, the microscopic molecular motion slows down, which leads to a less macroscopic relaxation during the same time period. Therefore, the temperature decrease and strain rate increase are equivalent on microscopic molecular motion behavior as well as on macroscopic viscoelastic behavior.

If a material possesses such an equivalence, it means that shifting the curves of the mechanical quantities along the logarithmic time axis rightward, i.e. decelerating the test speeds, has the same results as testing at higher temperatures, and vice versa. It can be illustrated in Fig. 17. We can select a specific temperature (T_2 in Fig. 17) as the reference temperature T_0, and plot the curves of a particular mechanical quantity at different temperatures with respect to logarithmic time, as shown in Fig. 17(a). If we shift them along the axis with a certain distance, denoted as $\lg a_T(T)$, then all these curves are able to join to the curve at T_0, and all curves are synthesized as a single curve, i.e. master curve, as shown in Fig. 17(b). The new independent variable after shifting is defined as the reduced time t_{red}, as shown in Eq. 2:

$$\lg t_{\mathrm{red}} := \lg t - \lg a_T \tag{2a}$$

$$or \quad t_{\mathrm{red}} := \frac{t}{a_T} \tag{2b}$$

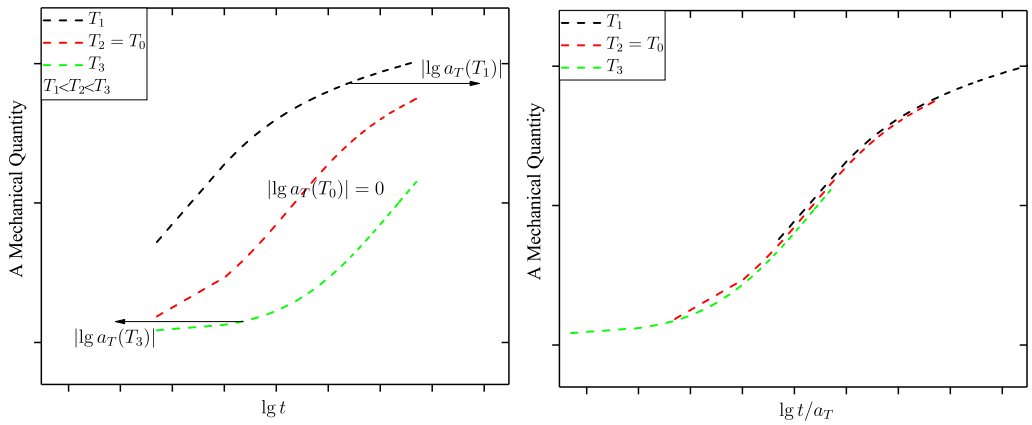

Figure 17. Schematics of the time-temperature superposition. (a) before applying the time-temperature superposition, (b) after applying the time-temperature superposition.

here, a_T is called shift factor, which is a decrease function of the absolute temperature. The function is dependent on T_0. The relationship Eq. 2 can also be transformed into a strain rate form as Eq. 3:

$$\dot{\varepsilon}_{\text{red}} := \frac{\mathrm{d}\varepsilon}{\mathrm{d}t_{\text{red}}} = \frac{\mathrm{d}\varepsilon}{\mathrm{d}t}\frac{\mathrm{d}t}{\mathrm{d}t_{\text{red}}} = a_T\dot{\varepsilon} \tag{3}$$

where $\dot{\varepsilon}_{\text{red}}$ denotes reduced strain rate. Note that in strain rate form, the shifting direction is the opposite of that in time form.

Regarding a certain mechanical quantity $F = F(T, \dot{\varepsilon})$, the shifting relationship can be expressed as:

$$F(T, \dot{\varepsilon}) = F(T_0, \dot{\varepsilon}_{\text{red}}) = F(T_0, a_T\dot{\varepsilon}) \tag{4}$$

This shift relationship is known as the time-temperature superposition (TTS) principle [30]. Based on the TTS principle, temperature and strain rate can be reduced into one variable, $\dot{\varepsilon}_{\text{red}}$. The same $\dot{\varepsilon}_{\text{red}}$ means the same mechanical response.

The TTS principle should be determined by finding the shift factor function which fits all the mechanical quantities well. The TTS principle has been applied successfully in some works of polyurethane using the Williams-Landel-Ferry Equation (WLF) equation such as [31]. Even so, we find that a linear function can fit a_T well for high strain rate tensile tests. In this study,

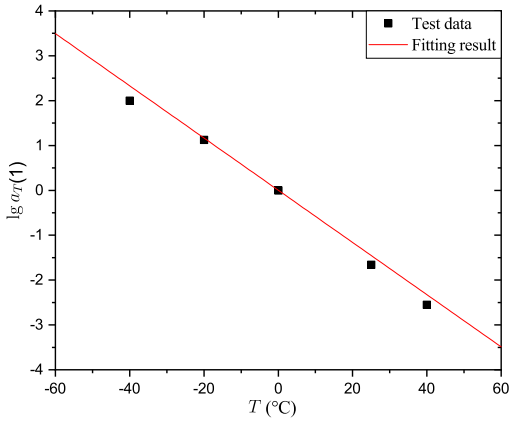

Figure 18. Fitting for $\lg a_T(T)$.

we take $T_0 = 273.15$ K (0°C) as the reference temperature, and determine the shifting amount a_T which can assemble curves at different temperatures into a smooth master curve. By fitting the value of a_T with a linear function as shown in Fig. 18, we get:

$$\lg a_T(T) = -0.0582(T - T_0) = 15.9 - 0.0582T \tag{5}$$

The fitness of this equation can be verified in the following sections.

4.2. Pre-failure behaviors

In this section, the mechanical quantities before failure are discussed. In Fig. 16, it can be observed that there are several stages in the stress-strain curve before failure. At the beginning stage, there is a linear segment at a small strain with a relatively stiff modulus. Then a nonlinear yield-like stage with a local peak follows. For some of the higher strain rate tests or lower temperature tests, after the peak value, the stress drops to a local valley. Finally, it enters a linear stress flowing or hardening stage with much lower modulus than the initial linear stage. These stages are measured by four mechanical quantities, i.e. initial modulus, pseudo yield stress, pseudo lower yield stress and secondary modulus in sequence. The initial modulus is calculated by dividing the stress value by corresponding strain in the initial linear section. The data of pseudo yield stress is fetched at the pseudo yield point, which is the turning point or the local peak of the curve. The corresponding strain is around 0.16 as shown in Fig. 19(a). For simplicity, we define roughly $\varepsilon_Y = 0.16$. Similarly, we define the strain of the pseudo

lower yield point $\varepsilon_{\mathrm{Yl}} = 0.6$ according to the curves that exhibited the local valley value, as shown in Fig. 19(b). Then we fetch the data at this strain to be the pseudo lower yield stress. The slope of the linear segment after the nonlinear stage is taken as the secondary modulus. Note that the post-yield and the pre-failure linear stage is a nonlinear stage when depicted in the true stress-strain curve.

In our analysis, the TTS principle is adopted according to Sec. 3.2.3 and Sec. 4.1. Besides time-temperature equivalence, the mechanical quantities can also depend directly on temperature and density [30, 32]. Remember that polyurethane is nearly incompressible, so the density remains constant. Just taking the additional direct influence of temperature in to account, $F = F(T, \dot{\varepsilon})$ in Eq. 4 can be corrected as:

$$F_{\mathrm{c}} := F(T_0, a_T\dot{\varepsilon}) = \frac{T_0}{T}F(T, \dot{\varepsilon}) \tag{6}$$

where T is in absolute unit, and F_c denotes the corrected mechanical quantity. The corrected values with respect to the reduce strain rate are potted in scatter in Fig. 20, respectively. In each figure, scatters can be synthesized in a smooth line, indicating the efficacy of Eq. 5.

Richeton et al. [33] adopted an inverse hyperbolic sine function combining the TTS principle to describe the yield stress of some polymers above the glass transition temperature. In this study, a simplified inverse hyperbolic sine function with four parameters is adopted to fit the initial modulus E, the pseudo yield stress σ_{Y} and the pseudo lower yield stress σ_{Yl}:

$$F_{\mathrm{c}} = C_1 \sinh^{-1}\left(C_2\left(\frac{\dot{\varepsilon}_{\mathrm{red}}}{\dot{\varepsilon}_0}\right)^{C_3}\right) + C_0 \tag{7}$$

We consider that the pseudo yield stress and the secondary modulus E_{H} increased with the increase of reduced strain rate. But when the pseudo yield stress level increases greater than the post-yield stress, the pseudo lower yield point appears, and the secondary modulus begins to decrease. Therefore, one more parameter C_4 is added to embody this character:

$$F_{\mathrm{c}} = C_1 \sinh^{-1}\left(C_2\left(\frac{\dot{\varepsilon}_{\mathrm{red}}}{\dot{\varepsilon}_0}\right)^{C_3}\right) + C_0 - C_4 \cdot \sigma_{\mathrm{y}} \tag{8}$$

In Eq. 7 and Eq. 8, C_0, C_1, C_2, C_3 and C_4 denote the material parameters to be determined by fitting the experimental data, In Eq. 8, σ_{y} is based

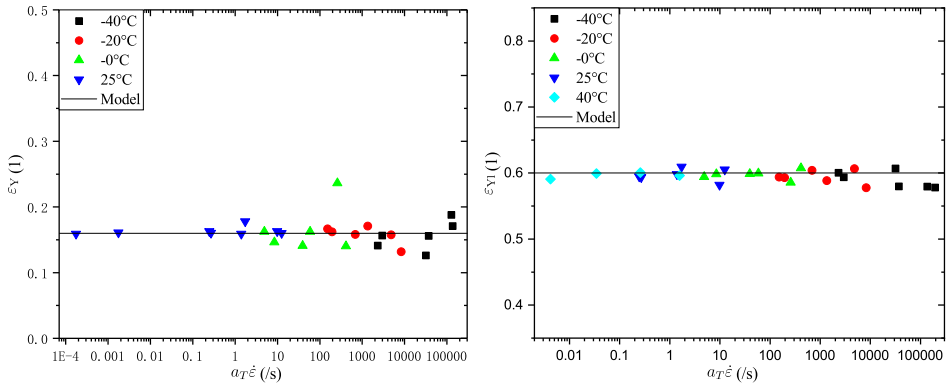

(a) (b)

Figure 19. Pseudo upper and lower yield strains. (a) upper yield strain,(a) lower yield strain.

on the measured value. The dependent variable F_c denotes the corrected mechanical quantities, i.e. initial modulus and yield stress in Eq. 7 and secondary modulus in Eq. 8. $\dot{\varepsilon}_{red}$ denotes the reduced strain rate, and $\dot{\varepsilon}_0$ denotes a reference reduced strain rate. Here we take $\dot{\varepsilon}_0 = 1$ /s for simplicity. σ_y denotes the pseudo yield stress in Eq. 8.

Results of the fitting parameters for the initial modulus, pseudo (upper) yield stress, pseudo lower yield stress, and secondary modulus are shown in Tab. 1. Fig. 20 plots the fitting master curve in full line. The results show that the formula can fit the data well with acceptable deviation for the initial modulus and the yield stress. The secondary modulus is not so accurate as the former two mechanical quantities. Nevertheless, it provides us the overview of large deformation behavior after the pseudo yield point.

Table 1: Fitting parameters of the pre-fracture behaviors

	C_0 (MPa)	C_1 (MPa)	C_2 (1)	C_3 (1)	C_4 (1)
Initial modulus	14.9	180	0.0820	0.569	—
Pseudo yield stress	1.38	17.6	0.102	0.480	—
Pseudo lower yield stress	2.48	14.4	0.242	0.402	—
Secondary modulus	0.322	2.60	263	0.5	−8.11

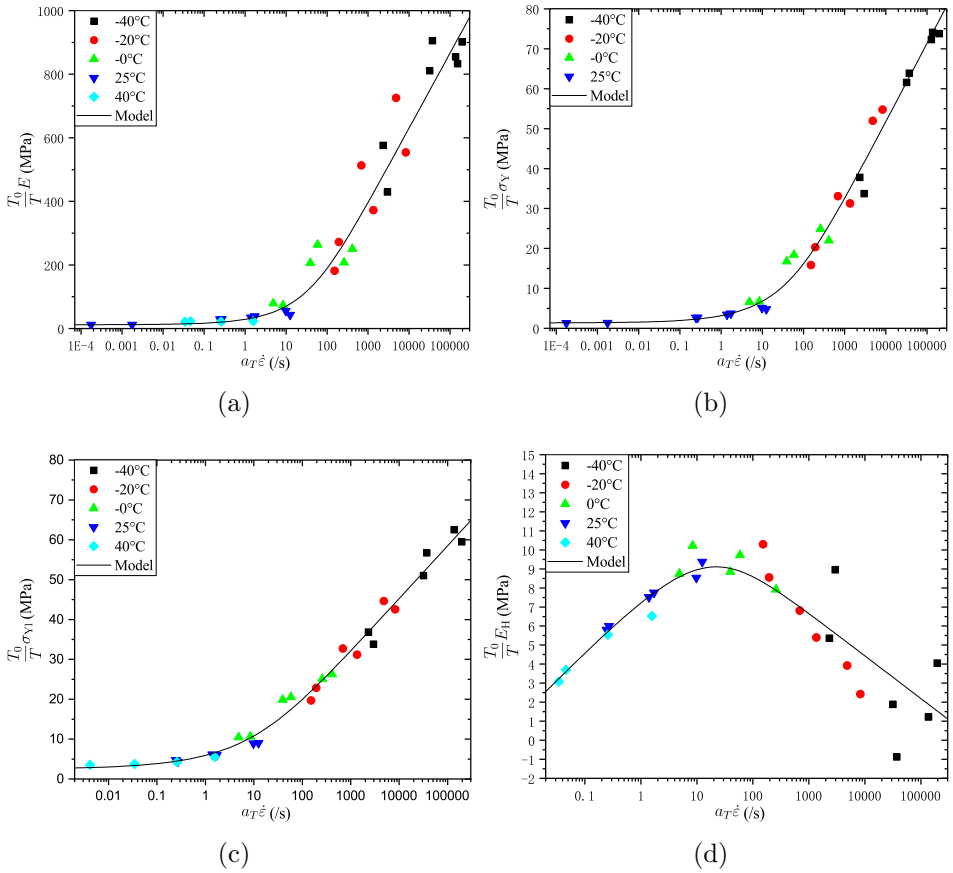

Figure 20. Master curve of mechanical quantities. (a) initial modulus, (b) pseudo yield stress, (c) pseudo lower stress, (d) secondary modulus.

4.3. Failure point

In this study, all specimens in intermediate strain rate tests underwent large deformation and then failed. According to the images captured by the camera, there was no observed necking since polyurethane is not plastic material. Most of our specimens were torn apart within the gauge section, as shown in Fig. 21, which verified the effectiveness of the dumbbell shape design. Comparison between the long specimens and the short ones shows that they have distinct different failure strength and failure elongation. That was because of the different stress concentration level on the arc section with different curvature. Therefore, long and short specimens are discussed separately. Note that one type of material should only possess one set of material constants. In this case, we obtained different fitting parameters as the data originate both from short and long specimens. Hence, the data account not only for material behaviors but also include dimensional influence. Accurate material constants can be acquired if the dimensional effect can be eliminated.

After applying the TTS principle, it can be found that both the failure strength and the failure elongation obeyed a linear law with respect to the logarithm reduced strain rate as shown in Fig. 22(a) and Fig. 23(a). Here, a simple fitting function can be put forward as follow:

$$\sigma_{\mathrm{s}} = \sigma_{\mathrm{s1}} \lg\left(\frac{\dot{\varepsilon}_{\mathrm{red}}}{\dot{\varepsilon}_0}\right) + \sigma_{\mathrm{s0}} \tag{9a}$$

$$\varepsilon_{\mathrm{s}} = -\varepsilon_{\mathrm{s1}} \lg\left(\frac{\dot{\varepsilon}_{\mathrm{red}}}{\dot{\varepsilon}_0}\right) + \varepsilon_{\mathrm{s0}} \tag{9b}$$

where σ_{s} and ε_{s} are tensile strength and ultimate elongation, respectively. σ_{s0}, σ_{s1}, $\varepsilon_{\mathrm{s0}}$, $\varepsilon_{\mathrm{s1}}$ are undetermined parameters. $\dot{\varepsilon}_{\mathrm{red}}$ denotes the reduced strain rate, and $\dot{\varepsilon}_0$ denotes a reference reduced strain rate. Here we also take $\dot{\varepsilon}_0 = 1$ /s for simplicity. The identified fitting parameters are in Tab. 2.

The fitting results of Eq. 9 for the long specimens are depicted in Fig. 22 and Fig. 23. In Fig. 22(a) and Fig. 23(a), the fitting results are in full lines. Inversely using Eq. 6, we can decompose the reduced strain rate into two variables, i.e. temperature and strain rate. Then the fitting function corresponds to a surface in temperature and strain rate space as shown in Fig. 22(b) and Fig. 23(b).

Eliminating the same independent variables $\dot{\varepsilon}_{\mathrm{red}}$ of the two equations in

Figure 21. A specimen after failure.

Table 2: Fitting parameters of tensile strength and ultimate elongation

	σ_{s0} (MPa)	σ_{s1} (MPa)	ε_{s0} (1)	ε_{s1} (1)
long specimen	24.66077	5.63601	3.07882	−0.20481
short specimen	21.15751	5.9246	2.56811	−0.19197

Eq. 9, we have:

$$\sigma_s = -\frac{\sigma_{s1}}{\varepsilon_{s1}}\varepsilon_s + \left(\sigma_{s0} + \sigma_{s1}\frac{\varepsilon_{s0}}{\varepsilon_{s1}}\right) \tag{10}$$

It means that at any strain rate and temperature, the failure points fall on a straight line in engineering stress-strain coordination. As shown in Fig. 24(a), the red dash line and the black full line represent the fitting results of failure points for short specimens and long specimens, respectively. These two straight lines can be regarded as the failure criterion. The black and the red scatters stand for the experimental results of failure points for long and short specimens, respectively. The dotted lines denote testing stress-strain results of the long specimens at certain temperatures and strain rates. Although the scatter data of failure point for each kind of specimens fluctuates owing to the unpredictable micro polymeric structure, manufacturing deficiency, and machining error, we find that the failure criteria for the long specimens are consistent with the scatter data quite well, while the short specimen has slightly larger deviation.

It is obvious that the tensile strength and ultimate elongation of the long specimens are larger than those of the short specimens, which indicates that the design of the long specimens successfully mitigated stress concentration and improved the test accuracy. Interestingly, the long and the short specimens have nearly the same values of both σ_{s1} and ε_{s1}, as shown in Tab. 2. It means that the slopes of the failure criterion of both kinds of specimens are nearly parallel, as shown in Fig. 24(a). Meanwhile, the offset between the two failure criterion indicates the existence of stress concentration. Therefore, the discrepancies of the σ_{s0} and ε_{s0} in two type of specimens indicate the existence of stress concentration. If the stress concentration is eliminated, then we can obtain accurate constants σ_{s0} and ε_{s0} of the material. Here,

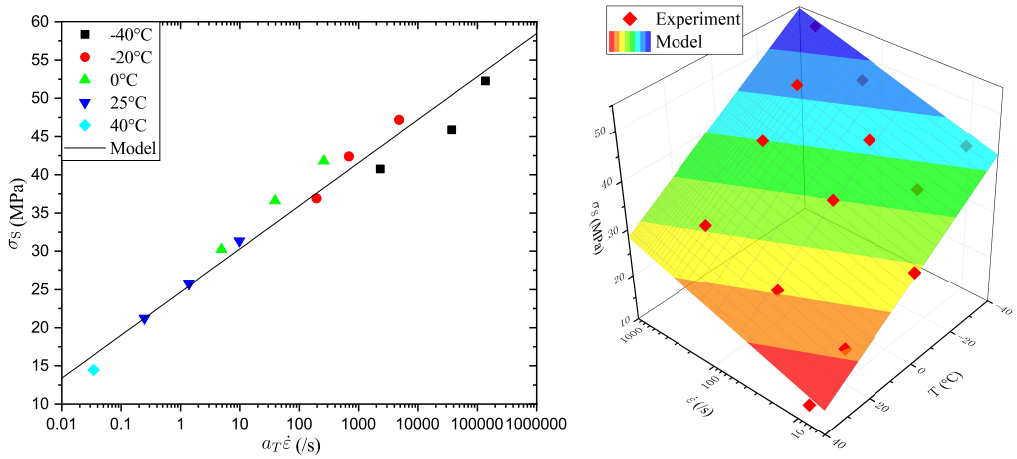

(a) (b)

Figure 22. Tensile strength for the long specimen. (a) master curve, (b) fitting surface.

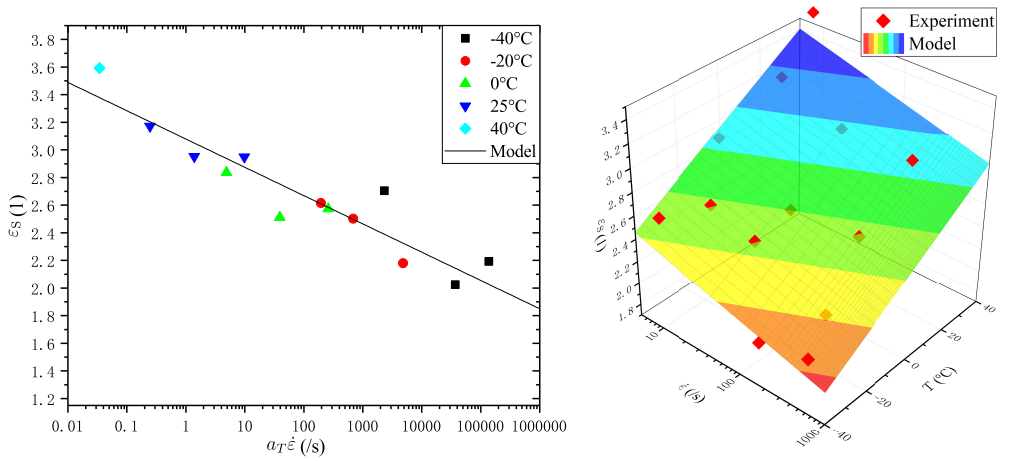

(a) (b)

Figure 23. Ultimate elongation for the long specimen. (a) master curve, (b) fitting surface.

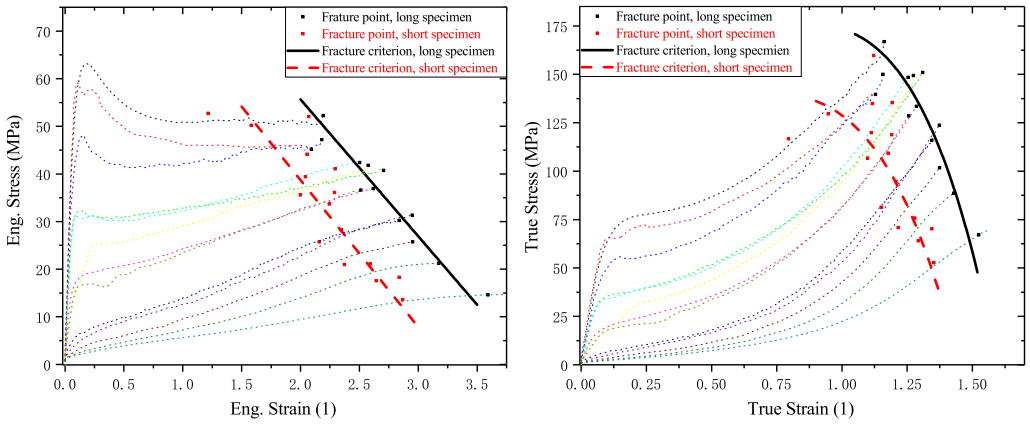

(a) (b)

Figure 24. Failure criterion. (a) engineering stress-strain, (b) true stress-strain.

since the longer specimens have less stress concentration, we consider the corresponding fitting results are closer to the viable value than the shorter one.

If we substitute Eq. 10 into Eq. 1, the failure criteria in true stress and true strain can be obtained as Eq. 11:

$$\sigma_{\mathrm{s}}^{\mathrm{true}} = -\frac{\sigma_{\mathrm{s1}}}{\varepsilon_{\mathrm{s1}}} \mathrm{e}^{2\varepsilon_{\mathrm{s}}^{\mathrm{true}}} + \left(\sigma_{\mathrm{s0}} + (\varepsilon_{\mathrm{s0}} - 1) \frac{\sigma_{\mathrm{s1}}}{\varepsilon_{\mathrm{s1}}} \right) \mathrm{e}^{\varepsilon_{\mathrm{s}}^{\mathrm{true}}} \tag{11}$$

Here, $\sigma_{\mathrm{s}}^{\mathrm{true}}$ denotes the true failure stress and $\varepsilon_{\mathrm{s}}^{\mathrm{true}}$ denotes the true failure strain. The curves are shown in Fig. 24(b). In true stress-strain form, the failure criterion turns out to be nonlinear.

4.4. Specimen temperature rise

In the discussion above, the initial temperature is taken to represent the specimen temperature. However, thermal generation of specimens is involved during dynamic tensile loading [26, 34] since it is not an isothermal process as in quasi-static tests. For the reason that specimens were mounted inside the chamber, it could be a challenge to monitor the instant temperature field within the specimen directly. Therefore, in this section, a rough estimation of temperature rise will be discussed.

In order to calculate the temperature rise using our data, a constitutive relationship should be given which defines the proportion of reversible energy

storage and irreversible energy consumption while loading. At present, we can only provide a simple estimation under several assumptions: (1) assume that the tests are adiabatic (regardless of the heat convection); (2) assume that the material is hyper-viscoelastic; (3) assume that the energy generated in equilibrium path [6] (based on a low strain rate test at 0.01 /s from [23]) is the only contribution of reversible energy (regardless of the contribution in viscoelastic portion); (4) assume that stress level also changes with temperature following the simple rule as

$$\sigma_{\mathrm{eq}}(T) = \frac{T_0}{T}\sigma_{\mathrm{eq}}(T_0) \tag{12}$$

where σ_{eq}, T, and T_0 denote the equilibrium stress, the current temperature, and the reference temperature, respectively. Assumptions (1) and (2) render the estimation to be the upper limit of the temperature rise. By subtracting the equilibrium energy density ΔW_{eq} from the total energy density $\Delta W_{\mathrm{total}}$, we get the irreversible energy density ΔW_{irre}:

$$\Delta W_{\mathrm{irre}} = \Delta W_{\mathrm{total}} - \Delta W_{\mathrm{eq}} \tag{13}$$

where the energy density is the area below the stress-strain curve:

$$\Delta W(\varepsilon) = \int_0^{\varepsilon} \sigma \mathrm{d}\varepsilon \tag{14}$$

Under the adiabatic assumption, all the irreversible energy contributes to temperature rise:

$$\Delta T = \frac{\Delta W_{\mathrm{irre}}}{c\rho} \tag{15}$$

where $c = 1.7\ \mathrm{J\cdot g^{-1}K^{-1}}$ [35] is the specific heat, $\rho = 1180\ \mathrm{kg\cdot m^{-3}}$ mentioned at Sec. 2.1. The temperature rises at each specimen are shown in Tab. 3.

It shows that little temperature rise happens at the pseudo yield point and the lower pseudo yield point, while the increase is more significant at the failure point. Then we fit the master curves based on the instant temperature. The correspondent parameters are shown in Tab. 4.

At the early stages of loading, the strains are relatively small, and therefore little irreversible energy is consumed to increase the temperature. Comparing Tab. 4 with Tab. 1, the results of the yield point and the lower yield point are similar. It means that taking the initial temperature for the calibration of the initial modulus is valid. By contrast, the failure points are at

Table 3: Temperature rise (°C)

	-40°C 639 /s	-40°C 173 /s	-40°C 10.9 /s	-20°C 329 /s	-20°C 46.9 /s	-20°C 13.3 /s	
Yield Point	3.373	2.999	1.804	2.447	1.729	1.001	
Lower Yield Point	14.832	13.695	7.577	10.851	7.610	4.746	
Failure Point	48.322	41.993	37.788	39.433	35.602	28.085	
	0°C 259 /s	0°C 39.3 /s	0°C 4.88 /s	25°C 280 /s	25°C 39.8 /s	25°C 7.02 /s	40°C 7.35 /s
Yield Point	1.007	0.869	0.348	0.238	0.168	0.119	0.09422
Lower Yield Point	5.745	4.130	1.949	1.654	1.087	0.252	0.52142
Failure Point	32.651	25.760	19.780	20.044	14.953	12.566	9.53245

Table 4: Fitting parameters on account of temperature rise(°C)

	C_0(MPa)	C_1(MPa)	C_2(1)	C_3(1)
Pseudo yield stress	1.80781	15.00409	0.10482	0.5641
Pseudo lower yield stress	2.88448	15.85789	0.2056	0.47972

	σ_{s0}(MPa)	σ_{s1}(MPa)	ε_{s0}(1)	ε_{s1}(1)
Failure Point	33.17413	8.2554	2.78252	−0.31646

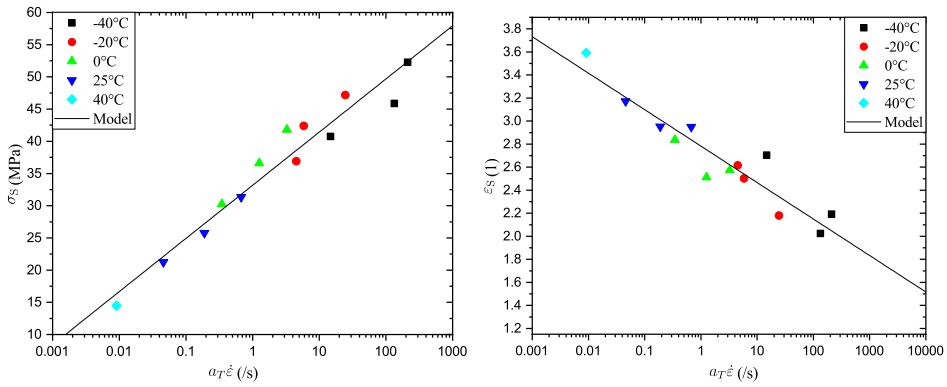

Figure 25. Maser curve of failure point considering temperature rise. (a) tensile strength, (b) ultimate strain.

much larger strains. As a result, the differences of parameters between Tab. 4 and Tab. 2 are more appreciable. The master curves of the failure point in consideration of temperature rise, which still fit the data well as shown in Fig. 25, possess narrower ranges of the reduced strain rate compared with Fig. 22(a) and Fig. 23(a). With the increase of strain rates or the decrease of initial temperatures, the specimen temperature rises at large strain increase significantly, which may be the cause of the up and down trend of the secondary modulus.

5. Conclusions

In this study, tensile behaviors of transparent polyurethane were examined. Quasi-static tests were conducted to verify the cyclic properties including the hysteresis, the softening and the equilibrium path. The results show that polyurethane is a typical viscoelastic material. Systematical investigations on intermediate strain rate tensile failure tests were carried out successfully with the help of a servo-hydraulic dynamic tensile test machine and the DIC technique with good accuracy. These intermediate strain rate tests fill the vacancy of intermediate strain rate tests that conventional apparatus could not cover, and provide direct data for analysis of impact loading on laminated glass. It is shown that transparent polyurethane has a strong temperature and strain rate dependence. With the decrease of temperatures or increase of strain rates, polyurethane exhibits the transition from

rubber-like behavior to glass-like behavior. Characteristic mechanical quantities including initial modulus, pseudo yield stress and strain, pseudo lower yield stress and strain, secondary modulus, tensile strength, and ultimate elongation are fitted with good agreement using the TTS principle and selected empirical functions. All these mechanical quantities can be described with smooth master curves, indicating the successful application of the TTS principle and identified the equivalence of temperature and strain rate effect. It is also interesting that the failure criterion is a linear line.

In this study, we adopted a phenomenological analysis. In our forthcoming works, a physical-based thermo-viscoelastic constitutive model of transparent polyurethane will be developed for better application of engineering analysis and structure simulations. We have mentioned in Sec. 4.4 that specimens experience temperature rise during loading and we have provide an rough estimation. Actual temperature changes has yet to be measured. Also, most material tests inevitably include certain structure effects such as triaxial stress state and wave transmission. Hence numerical tests can be conducted to simulate the thermal and structural effect and assist developing the constitutive model. The temperature dependence and strain rate dependence at low strain rate are not fully clear at present. Thus quasi-static tests including tensile failure tests and cyclic tests at various temperatures and strain rates will be carried out. These tests can provide supplementary data for developing constitutive models at large strains.

6. Acknowledgements

This work was partially supported by the National Natural Science Foundation of China (Nos. 11672110, 11472110 and 11372113), Natural Science Foundation of Guangdong Province (No. 2017A030313014), and the opening project of State Key Laboratory for Strength and Vibration of Mechanical Structures (Xi'an Jiaotong University) (No.SV2017-KF-04). We also thank the experimental support from KINGFA Ltd.

7. References

[1] R. Dolbeer, S. E. Wright, J. R. Weller, A. L. Anderson, M. J. Beiger, Wildlife strikes to civil aircraft in the united states, 1990-2014, Bird Strikes.

[2] M. Larcher, G. Solomos, F. Casadei, N. Gebbeken, Experimental and numerical investigations of laminated glass subjected to blast loading, International Journal of Impact Engineering 39 (1) (2012) 42–50. doi:10.1016/j.ijimpeng.2011.09.006.

[3] X. Zhang, H. Hao, Y. Shi, J. Cui, The mechanical properties of polyvinyl butyral (PVB) at high strain rates, Construction and Building Materials 93 (2015) 404–415. doi:10.1016/j.conbuildmat.2015.04.057.

[4] S. R. Ledbetter, A. R. Walker, A. P. Keiller, Structural use of glass, Journal of Architectural Engineering 12 (3) (2006) 137–149. doi:10.1061/(ASCE)1076-0431(2006)12:3(137).

[5] R. A. Behr, J. E. Minor, H. S. Norville, Structural behavior of architectural laminated glass, Journal of Structural Engineering 119 (1) (1993) 202–222. doi:10.1061/(ASCE)0733-9445(1993)119:1(202).

[6] H. Qi, M. Boyce, Stress–strain behavior of thermoplastic polyurethanes, Mechanics of Materials 37 (8) (2005) 817–839. doi:10.1016/j.mechmat.2004.08.001.

[7] G. Oertel, Polyurethane handbook : chemistry, raw materials, processing, application, properties, Hanser Publishers, 1985.

[8] J. Blackwell, K. H. Gardner, Structure of the hard segments in polyurethane elastomers, Polymer 20 (1) (1979) 13 – 17. doi:10.1016/0032-3861(79)90035-1.

[9] K. Holzworth, Z. Jia, A. Amirkhizi, J. Qiao, S. Nemat-Nasser, Effect of isocyanate content on thermal and mechanical properties of polyurea, Polymer 54 (12) (2013) 3079–3085. doi:10.1016/j.polymer.2013.03.067.

[10] D. Fragiadakis, R. Gamache, R. Bogoslovov, C. Roland, Segmental dynamics of polyurea: Effect of stoichiometry, Polymer 51 (1) (2010) 178–184. doi:10.1016/j.polymer.2009.11.028.

[11] X. hu Yao, Experimental investigation and numerical simulation on arc windshields of aircrafts subjected to bird impact, Master's thesis, Taiyuan University of Technology (2001).

[12] X. hu Yao, Q. Han, X. qing Zhang, L. ma Zhao, Experimental study on arc wind shield of fighter subjected to bird impact, Explosion and Shock Waves 25 (5) (2005) 417–422. doi:10.11883/1001-1455(2005)05-0417-06.

[13] A. Sharma, A. Shukla, R. A. Prosser, Mechanical characterization of soft materials using high speed photography and split hopkinson pressure bar technique, Journal of Materials Science 37 (5) (2002) 1005–1017. doi:10.1023/A:1014308216966.

[14] J. Yi, M. Boyce, G. Lee, E. Balizer, Large deformation rate-dependent stress–strain behavior of polyurea and polyurethanes, Polymer 47 (1) (2006) 319–329. doi:10.1016/j.polymer.2005.10.107.

[15] A. V. Amirkhizi, J. Isaacs, J. McGee, S. Nemat-Nasser, An experimentally-based viscoelastic constitutive model for polyurea, including pressure and temperature effects, Philosophical Magazine 86 (36) (2006) 5847–5866. doi:10.1080/14786430600833198.

[16] S. S. Sarva, S. Deschanel, M. C. Boyce, W. Chen, Stress–strain behavior of a polyurea and a polyurethane from low to high strain rates, Polymer 48 (8) (2007) 2208–2213. doi:10.1016/j.polymer.2007.02.058.

[17] J. Shim, D. Mohr, Using split hopkinson pressure bars to perform large strain compression tests on polyurea at low, intermediate and high strain rates, International Journal of Impact Engineering 36 (9) (2009) 1116–1127. doi:10.1016/j.ijimpeng.2008.12.010.

[18] M. Grujicic, R. Yavari, J. S. Snipes, S. Ramaswami, T. Jiao, R. J. Clifton, Experimental and computational study of the shearing resistance of polyurea at high pressures and high strain rates, Journal of Materials Engineering and Performance 24 (2) (2014) 778–798. doi:10.1007/s11665-014-1316-x.

[19] H. Guo, W. Guo, A. V. Amirkhizi, R. Zou, K. Yuan, Experimental investigation and modeling of mechanical behaviors of polyurea over wide ranges of strain rates and temperatures, Polymer Testing 53 (2016) 234–244. doi:10.1016/j.polymertesting.2016.06.004.

[20] R. G. Rinaldi, A. J. Hsieh, M. C. Boyce, Tunable microstructures and mechanical deformation in transparent poly(urethane urea)s, Journal

of Polymer Science Part B: Polymer Physics 49 (2) (2010) 123–135. doi:10.1002/polb.22128.

[21] R. G. Rinaldi, M. C. Boyce, S. J. Weigand, D. J. Londono, M. W. Guise, Microstructure evolution during tensile loading histories of a polyurea, Journal of Polymer Science Part B: Polymer Physics 49 (23) (2011) 1660–1671. doi:10.1002/polb.22352.

[22] J. Fan, J. Weerheijm, L. Sluys, High-strain-rate tensile mechanical response of a polyurethane elastomeric material, Polymer 65 (2015) 72–80. doi:10.1016/j.polymer.2015.03.046.

[23] L. Zhang, X. Yao, S. Zang, Q. Han, Temperature and strain rate dependent tensile behavior of a transparent polyurethane interlayer, Materials & Design (1980-2015) 65 (2015) 1181–1188. doi:10.1016/j.matdes.2014.08.054.

[24] C. Roland, J. Twigg, Y. Vu, P. Mott, High strain rate mechanical behavior of polyurea, Polymer 48 (2) (2007) 574–578. doi:10.1016/j.polymer.2006.11.051.

[25] S. Raman, T. Ngo, J. Lu, P. Mendis, Experimental investigation on the tensile behavior of polyurea at high strain rates, Materials & Design 50 (2013) 124–129. doi:10.1016/j.matdes.2013.02.063.

[26] P. Mott, C. Giller, D. Fragiadakis, D. Rosenberg, C. Roland, Deformation of polyurea: Where does the energy go?, Polymer 105 (2016) 227–233. doi:10.1016/j.polymer.2016.10.029.

[27] L. Zhang, X. Zhang, X. Yao, S. Zang, Experimental investigation on the tensile behavior of a transparent polyurethane interlayer, International Journal of Materials Research 106 (9) (2015) 996–1001. doi:10.3139/146.111267.

[28] L. Mullins, N. R. Tobin, Stress softening in rubber vulcanizates. part i. use of a strain amplification factor to describe the elastic behavior of fillerreinforced vulcanized rubber, Journal of Applied Polymer Science 9 (9) (1965) 2993–3009. doi:10.1002/app.1965.070090906.

[29] M. Hossain, D. K. Vu, P. Steinmann, Experimental study and numerical modelling of VHB 4910 polymer, Computational Materials Science 59 (2012) 65–74. doi:10.1016/j.commatsci.2012.02.027.

[30] J. D. Ferry, S. A. Rice, Viscoelastic properties of polymers, 3rd Edition, Wiley, 1980.

[31] P. J. van Ekeren, E. P. Carton, Polyurethanes for potential use in transparent armour investigated using DSC and DMA, Journal of Thermal Analysis and Calorimetry 105 (2) (2011) 591–598. doi:10.1007/s10973-011-1665-8.

[32] J. Qiao, A. V. Amirkhizi, K. Schaaf, S. Nemat-Nasser, G. Wu, Dynamic mechanical and ultrasonic properties of polyurea, Mechanics of Materials 43 (10) (2011) 598–607. doi:10.1016/j.mechmat.2011.06.012.

[33] J. Richeton, S. Ahzi, K. Vecchio, F. Jiang, R. Adharapurapu, Influence of temperature and strain rate on the mechanical behavior of three amorphous polymers: Characterization and modeling of the compressive yield stress, International Journal of Solids and Structures 43 (7-8) (2006) 2318–2335. doi:10.1016/j.ijsolstr.2005.06.040.

[34] Z. Pan, J. Xiong, S. Liang, M. Zou, Transient deformation and heat generation of solid polyurethane under impact compression, Polymer Testing 61 (2017) 269–279. doi:10.1016/j.polymertesting.2017.05.033.

[35] Thermoplastic polyurethane elastomers elastollan product range, http://www.polyurethanes.basf.com/pu/solutions/en/function/conversions:/publish/content/group/News_und_Medien/Spezialelastomere/Thermoplastic_Polyurethane_Elastomers_Product_Range_EN.pdf, accessed: 2018-12-27.